Attachment 7

Evolution of seismic interpretation during the last three decades

Satinder Chopra, Arcis Seismic Solutions, Calgary
Kurt J. Marfurt, The University of Oklahoma, Norman

The ingredients of seismic interpretation include the right mix of geological and geophysical knowledge, together with a liberal dose of imagination, tempered with a considerable amount of patience. Seismic interpretation is a skill that one acquires with experience, but is constantly reinvigorated with new ideas and tools provided by younger university graduates. The prime ingredients for seismic interpretation are seismic reflection data coupled with a geologic depositional and tectonic model which together provide the framework for integrating borehole, microseismic, and production data resulting in a good reservoir model. Although commonly used in both engineering and environmental applications, most seismic reflection surveys are acquired for oil and gas exploration in both land and offshore areas around the world. Hydrocarbon accumulations are found at varying depths of a few thousand meters below the Earth's surface which are ultimately confirmed by drilling. Because the cost of drilling closely spaced wells can be prohibitively expensive, interpreted seismic data provide not only initial well locations in a wildcat environment, but also, when coupled statistically with production and well-log data, locations with higher probability of success in a resource play having hundreds of wells.

Early exploration efforts were aimed at using seismic reflection surveys to find large structural traps that could hold oil and gas, or to map one or more faults that may act as barriers to the flow of oil. Such seismic mapping led to the discovery of many large oil and gas fields around the world. Each decade has seen continuous improvement in seismic acquisition, processing, and interpretation, with today's exploration objectives much more subtle than mapping big bumps and faults.

In June 1982, SEG began publishing *TLE*, a table-top magazine meant to accompany the peer-reviewed archived journal Geophysics. Original expectations were that *TLE* would provide workflows, case studies, and best practices to practicing geophysicists, most of whom are interpreters. As *TLE* completes 30 years this month, the *TLE* Editorial Board suggested that we look back and assess how far we have come in doing seismic interpretation during the last three decades, and if possible, predict where we might be headed in the future. This is the motivation for this article.

Figure 1 is a timeline that shows at a glance the developments that took place in seismic interpretation from 1956 to 2008 (Liner, 2008).

Interpretation circa 1982

We pick up the threads from the year 1982 by assessing the state-of-the-art of seismic interpretation at that time. Since the beginning of the 20th century, most oil and gas companies focused on finding large structures (ideally) containing large amounts of oil. That trend continued into 1982, but with the easy structures already found in the lower 48 United States and many other places in the world, the search for elephants took place in either relatively unexplored countries or in harsher environments in previously explored countries. The principles of seismic stratigraphy introduced by Peter Vail and others in 1976 changed this paradigm by providing a framework to define, explore for, and exploit stratigraphic traps. Most seismic interpretation in the 1980s was still done using 2D seismic data. Although early three-dimensional (3D) seismic surveys were acquired in the mid-1970s, many if not most companies considered them to be an exploitation rather than an exploration tool.

In addition to being 2D, most seismic data in the early 1980s were interpreted on paper sections by hand using colored pencils. Major innovations unknown to today's tech-savvy students included not only the electric pencil sharpener, but also the electric eraser needed to change those bad picks. The seismic data available for land surveys had grown from 6 through 12 to 24 fold. The large amount of offshore seismic data being acquired in the early 1980s gave rise to a data explosion that prompted the need for more efficient ways of interpreting data. The second data explosion started as 3D

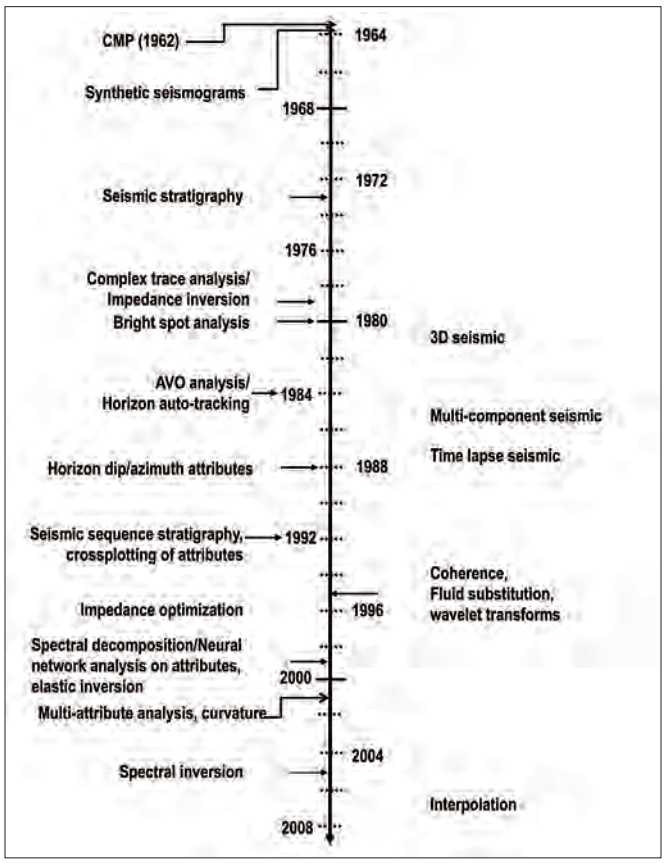

Figure 1. *Timeline showing developments in seismic interpretation. Modified from Liner (2008).*

seismic data began to pour in, fueling fears that interpreters with colored pencils in hand could not keep up. Fortunately, the geophysical and computer industries were tightly linked from the early 1950s. Seismic data in the 1980s were processed digitally on a device called a computer, which used to be the job title for a geophysicist who computed statics and velocity corrections. Once seismic processors began interactively selecting processing parameters and quality-controlling the resulting images, followed by picking statics, the move to interactive seismic interpretation was straightforward. Oil company research groups were engaged in interactive interpretation with mainframes and minicomputers about 1982, with commercial applications appearing in the market soon after. These interactive interpretation computers were called workstations and consisted of two or three large (measured in kg rather in pixels) computer monitors for displaying and mapping the data, together with a keyboard and some pointing devices such as a track ball, mouse, or stylus. Disk access was slow and disk storage was expensive. In the day of beta and VHS, the first 12-inch optical platter was introduced in 1984 and held 1 Gbyte of memory. You could write only once, so mistakes in data scaling were frowned upon. With two large friends, these workstations were quite portable and could be slid across the room.

Early interactive workstations started with variable-area and then wiggle-trace displays. Tektronix and other devices provided eight colors in the late 1970s, with the Genisco providing 16 colors in the mid-1980s. Color became pervasive, first for maps, then for recursive inversion to estimate relative acoustic impedance (Lavergne, 1975; Lindseth, 1976, 1979) and complex trace attributes (such as the envelope, instantaneous phase, and instantaneous frequency (Taner et al., 1979). Typically, these applications and plots were run as batch jobs on a mainframe or large minicomputer. With quick interaction, wavelet (also called response) and other trace attributes were introduced (Bodine, 1984, 1986), followed by interval attributes (Sonneland et al., 1989). Limitations in color depth were recognized in 1982. Knobloch (1982) used an image of Cheryl Tiegs (the cover girl of that year) to demonstrate the value of using thousands rather than dozens of colors.

For well-to-seismic ties, the log curves, usually supplied on paper, were digitized by hand and then processed to obtain CVL or synthetic seismogram plots on transparency paper or film. Such plots were attached to seismic paper sections to examine the correlation between the two. The final results of seismic interpretation were presented as structural contour and isopach maps. For the former, as well as the latter, the horizons and faults were colored on hardcopy seismic sections. An advance over posting these events and contouring them by hand was to have a technologist digitize the hardcopy interpretation and upload these picks to the mainframe for computer contouring. A major drawback of this innovation was that the forebearers of information technology people became involved. In many oil companies, special permission was required to change the picks in a database after they had been uploaded. Definitely not interactive!

In the early 1980s poststack time migration of 2D seismic data was available but was felt necessary to use only on structurally complex data. "True-amplitude" processing and bright spots, referring to strong isolated reflections and change in reflection character on seismic sections, were accepted and expected to be associated with gas accumulations. Using long-window automatic gain control (AGC) bright spots had significant impact in many areas, notably offshore Louisiana.

Bright spot association with gas was later confirmed in other areas, but interpreters soon realized that such bright reflections could also indicate hard streaks, volcanic intrusions, and coal beds.

The structural hydrocarbon trap of the early 1980s consisted of a permeable reservoir overlain by an impervious cap rock or seal that would prevent the escape of oil and gas. Using sequence stratigraphic principles communicated by Vail et al. (1977), explorationists began to recognize such stratigraphic traps in their seismic data as well. These traps were believed to be formed as a result of lateral changes in lithology or a break in continuity of the reservoir rock. Pinch outs, unconformities, reefs, sand lenses, or channel deposits are just some of the examples of early stratigraphic traps. Stratigraphic interpretation of 2D seismic during the 1980s was limited by vertical resolution and relatively low signal-to-noise ratios. Nevertheless, the seismic stratigraphy workflow enabled interpreters to make geologic time correlations, define depositional units in terms of their thickness and depositional environment, burial history, paleotopography, and so on. These approaches continued with the assimilation of 3D seismic volumes that provide data at fine spatial sampling leading to accurate 3D seismic imaging of the subsurface, thereby enabling interpreters to accurately estimate the thickness and areal extent of the features. The lateral resolution of 3D seismic data over conventional 2D was higher. More importantly, by eliminating "sideswipes" much of the ambiguity of tying horizons on 2D migrated dip lines to those on strike lines, as well as tracking individual faults, was eliminated. This trend toward attaining greater bandwidth continues. The challenge, though, is to have greater bandwidth yet retain the "true-amplitude" properties of the original data.

Interpretation and advances in seismic acquisition and processing

The ideal 2D seismic line runs perpendicular to geologic strike such that the bulk of seismic reflections come from within the 2D vertical plane of the line. In the more common, less-than-ideal situation, considerable out-of-the-plane energy comes from crossline dip and scatterers on either side of the 2D line. If the geologic structure is predominantly two-dimensional, a skilled interpreter can envision such out-of-the-plane effects and generate a good-quality time-structure map, including major faults, from horizons interpreted on a coarse grid (~500 m) of 2D seismic lines. However, even if the structure is 2D, the depositional environment is usually not, such that detailed stratigraphic features of interest are much more challenging, if not impossible to map from 2D data.

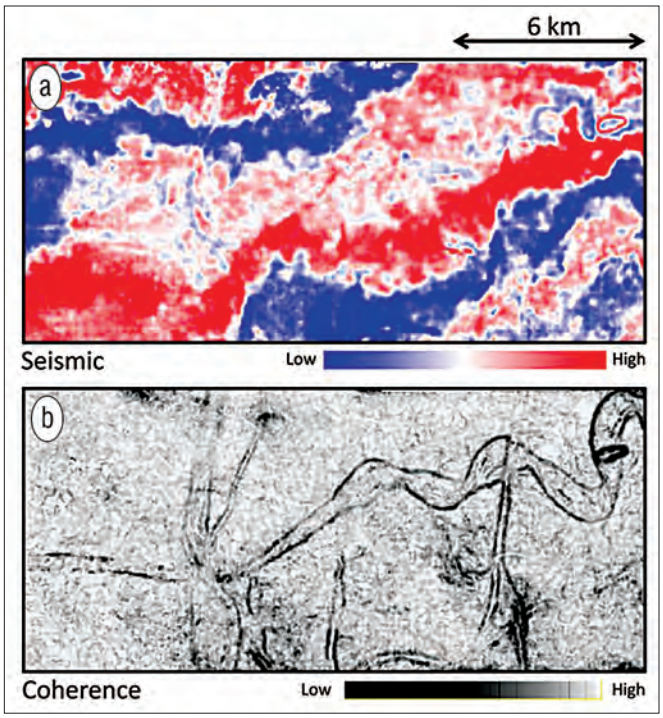

Figure 2. *Comparison of time slices (at 1333 ms) from (a) seismic and (b) coherence volumes. Notice the subtle channel signature is not clearly evident on the seismic data.*

Such limitations led to the development and, ultimately, the near wholesale adoption of 3D seismic data. The fine sampling in the inline and crossline directions in 3D seismic volumes leads to accurate 3D seismic imaging during processing, higher geometrical resolution and sharpened detail on the spatial distribution of lithologies, porosities, and fluids. Well-imaged 3D volumes can be used to generate vertical geologic sections in any direction. 3D seismic data not only enhance structural visualization, but enable improved stratigraphic interpretation as well.

Narrow azimuth to wide azimuths. Although early 3D seismic surveys densely sampled the subsurface, their aperture was so narrow that the subsurface image was influenced by the direction of shooting. Considerable work was devoted to determine "which azimuth" was best, with dip direction being more amenable to seismic imaging and strike direction more amenable to velocity analysis.

As 3D seismic became routine in the early 1990s, there was a steady increase in not only the quality but also the capacity of seismic recording. First the channel count increased from several hundreds to tens of thousands of channels. This made land 3D wide-azimuth acquisition possible. Similarly, the development of the ocean-bottom cable and later multiship acquisition provided wide-azimuth surveys in the marine data as well. The multitude of azimuths provided better statics solutions, better velocity analysis, greater leverage against coherent ground roll and multiples, and alternative subsurface illumination angles that together provided superior target images.

Growing interpretational needs have also driven advances in hardware development, acquisition, and processing. Wide-azimuth acquisition is critical to open-fracture detection and estimation of the magnitude and strike of maximum horizontal stress. In addition to providing greater leverage against multiples, long-offset data (defined as when the source-receiver offset exceeds the depth of the target) provide greater sensitivity to shear impedance, and in many cases, density, vertical-transverse isotropy and horizontal-transverse isotropy.

Modern slip-sweep vibrator technology provides a means of economically acquiring denser source points in areas with relatively easy access, providing a proper sampling of shallow diffractors, thereby improving the deeper image (Pramik, 2011).

Geophone hardware has also provided significant interpretation benefits. Piezoelectric and MEMs technology provide high-fidelity three-component and (at the seafloor) four-component recording, extending the bandwidth not only higher to increase resolution, but at the lower end as well, providing components needed for impedance inversion. Modern solid streamers have effectively eliminated the receiver ghost, thereby significantly broadening the seismic bandwidth.

Time migration. The term seismic migration refers to the process of mapping seismic reflections from their recorded positions to their true positions. A review of seismic migration requires an article at least as long as this one on interpretation. So, rather than summarize the development of migration from 1982, we limit ourselves to summarize its impact on interpreters. In 1982, seismic migration was recognized as being critical to interpreting seismic data over complex structure. Anticlines (and traps!) appear narrower and sharper, the lengths of reflector segments become shorter and moved updip, bow-tie patterns are collapsed into synclines, and diffractions are focused on edges thereby improving lateral resolution. Geometric spreading effects are more properly handled, improving amplitude fidelity.

Because of computational intensity, early migrations were applied to 2D stacked time sections with Kirchhoff (Schneider, 1978), finite-difference (Claerbout, 1976), Fourier transform (Stolt, 1978), and phase-shift (Gazdag, 1978) algorithms competing for market share. The finite-difference techniques had greater flexibility in handling more complicated velocity variations, but were limited to imaging dips less than (depending on the algorithm used) 15–60°. The Kirchhoff algorithms had the advantage of handling steep dips up to 90° and imaging data acquired with irregular shot and receiver spacing (not uncommon for land data). 2D prestack time migration provided improved results when refraction and other velocity effects gave rise to an inferior NMO correction and stack.

The mid-to-late 1980s saw these techniques becoming routine as interpreters realized that migration not only aided interpretation of complex structures, but also helped to focus onlap, offlap, toplap and other configurations key to the newly adopted seismic stratigraphy workflow. Nevertheless, interpreters encountered a new headache. While 2D dip and strike lines tie on the stacked section, they do not tie on 2D migrated sections, with the dip-line reflections moving updip

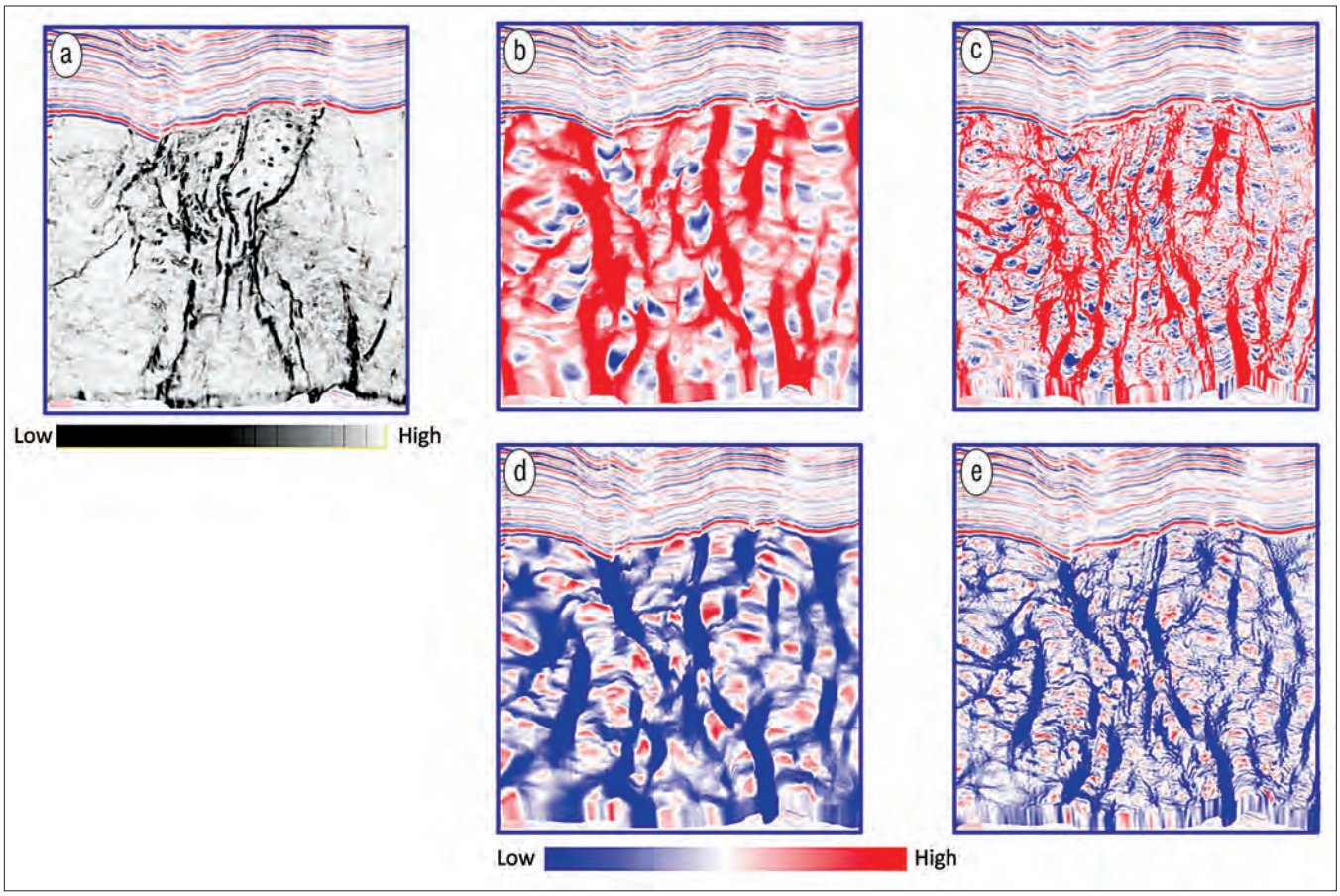

Figure 3. *Comparison of chair displays where the vertical section is a seismic inline and the horizon slice is from (a) coherence, (b) most-positive principal curvature (long-wavelength), (c)most-positive principal curvature (short-wavelength), (d) most-negative principal curvature (long-wavelength), and (e) most-negative principal curvature (short-wavelength). Notice the clarity with which the lineaments can be picked up on the coherence and the curvature horizon slices.*

and the strikeline reflections, appearing flat, staying in place. This gave rise to two rather unsatisfying workflows. The first was to vertically shift the strike lines to aid reflector tying across the survey. In steeply dipping areas, the picks on the strike lines were then discarded before generating a map. The second workflow was much more tedious—to pick the unmigrated, stacked data (which tied well), including bow ties and other crossing reflections, converting this multivalued function of x and y into single-valued patches and 3D map-migrating each patch to accumulate the result.

The 2D migration algorithms were easily generalized to 3D, but the computer requirements were extremely large. This computational demand resulted in most major oil companies entering the supercomputer world, investing in CDC 7600, Cray, and later Connection Machine computers that cost US $10–20 million. An early observation was that 3D Kirchhoff migration algorithms could easily be modified to produce a "target-oriented" image—either a desired subvolume or a decimated set of inlines and crosslines with a cost proportional to the size of the output. This latter capability had great value in migration-driven velocity analysis. In this workflow of the late 1980s, multiple migrations generating (target-oriented) output were run at percentages (e.g., 90%, 95, 100, 105, and 110%) of the "migration velocity" obtained from conventional stacking analysis. Long rolls of hardcopies were often rolled down the hall, with the interpreter marking which velocity best focused a reflection-fault intersection in a given image. These observations were used to update the velocity model after which the entire volume was migrated.

Depth migration. Often the geologic overburden has significant lateral variation of velocity associated with complex folding, submarine canyons, faulted subsurface layers, salt diapirism, shallow carbonate reefs, unevenly distributed glacial till not handled by refraction statics and anhydrite dissolution. In such cases, none of the time-migration algorithms accurately image the scattered energy to the proper position. Given an accurate depth model, depth migration not only places events at their correct lateral position, removes velocity pull-up and push-down effects including fault shadows, enables calculation of more accurate volumetrics, but also improves the vertical and lateral resolution by more properly aligning events along a deformed, possibly multivalued, hyperbola. The quality of a depth migration is only as good as the quality of the input interval velocity-depth model. Such an accurate velocity model can be used for other applications including acoustic impedance inversion, AVO analysis, and pore pressure prediction.

When originally introduced, many interpreters were an-

noyed by the change in waveform produced by depth migrations. Seismic stratigraphers form a library of waveforms and interference patterns in their minds that represent sometimes subtle changes. Where in time migration a consistent waveform persisted along a horizon going from shale on shale to shale on carbonate, in depth migration the waveform was stretched in the higher-velocity zone. If the velocity model was accurate, the deeper part of the waveform would be stretched in the carbonate and upper part of the waveform unstretched in the shale, giving rise to an asymmetrical waveform. Inaccurate velocity models generated even more complicated stretch and squeeze patterns. Herron (2000) addresses some of the interpretation pitfalls of depth-migrated images generated using an inaccurate velocity model.

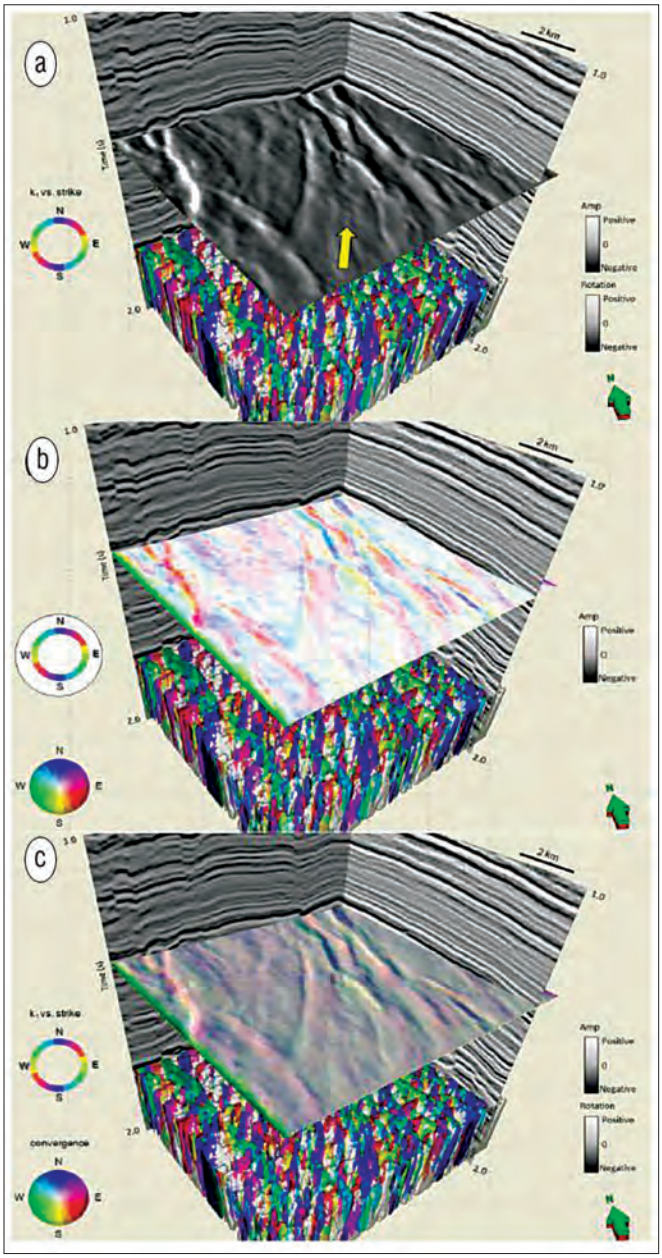

Figure 4. *Time slice at* t = *1.330 s (a) Through the volume of reflector rotation about the average reflector normal. We interpret the cross-hatched pattern indicated by the yellow arrow as either an indication of rotation about antithetic faults, or a suite of relay ramps. (b) The volume of the reflector convergence volume displayed using a 2D color wheel. Blue indicates reflectors pinching out to the north, red to the southeast, and cyan to the northwest. (c) The corendered volume of reflector convergence displayed using a 2D color wheel and reflector rotation displayed using a gray scale and 50% transparency. We interpret the thickening and thinning of the reflectors to be controlled by the rotating fault blocks. Below the time slice, we show a box probe view of the most-positive principal curvature lineaments displayed in 3D with the more planar features rendered transparent.*

Interpreters were also annoyed that the significantly more expensive so-called "depth" migration did not properly tie their wells. Furthermore, steeply dipping fault-plane reflections did not abut but rather crossed reflection terminations associated with the fault. The importance of velocity anisotropy in imaging was discovered.

By the late 1980s, 3D poststack depth imaging had become routine. Over the last decade or so, 3D prestack depth imaging has also become routine. Algorithms that correctly account for flat or steeply dipping ("tilted") velocity anisotropy associated with shales and thin bedding, as well as azimuthal anisotropy associated with fractures and nonuniform horizontal stress are offered by all the major service companies. Unfortunately, the headaches of the 1980s map migration have been replaced by the headaches of carefully generating velocity-depth models including rugose salt. As with map migration, such work is done by interpreters, rather than by seismic processors. Thus, the tedium (and employment opportunities) of migration has persisted for two generations.

Prestack image gathers. The debate of whether or not depth migration or time migration is appropriate or advantageous is not always the most important question in imaging. Elastic and azimuthal studies require analysis of prestack images (or image gathers). Many interpreters perform prestack migration only because they know they must eventually engage in elastic and azimuthal interpretation; the value of the migration is then primarily in the image gather. Allen et al. (1995) and Mosher et al. (1996) demonstrated the importance of performing migration on properly imaged gathers.

Interpretation and seismic attributes

By the early 1980s, almost all seismic surveys were migrated (with 2D complex structures being migrated in depth). In addition to generating structure and thickness maps, many interpreters adopted the seismic stratigraphy workflows introduced by Peter Vail, Bob Sheriff, and Tury Taner in 1977. It was quickly realized that not all high-amplitude anomalies were "bright spots" associated with gas accumulations, but could also be caused by igneous intrusions, carbonate streaks, and coal beds. Long-window automatic gain control provided a means to sufficiently balance the data for display, yet preserve local amplitude anomalies. Minicomputers and mainframes both provided interactive capabilities, as well as simple 8- and 16-color display capabilities. Almost every major oil company started developing interactive interpretation applications—picking, autotracking, mapping, volumetrics, and simple attributes. The success of AVO in extending

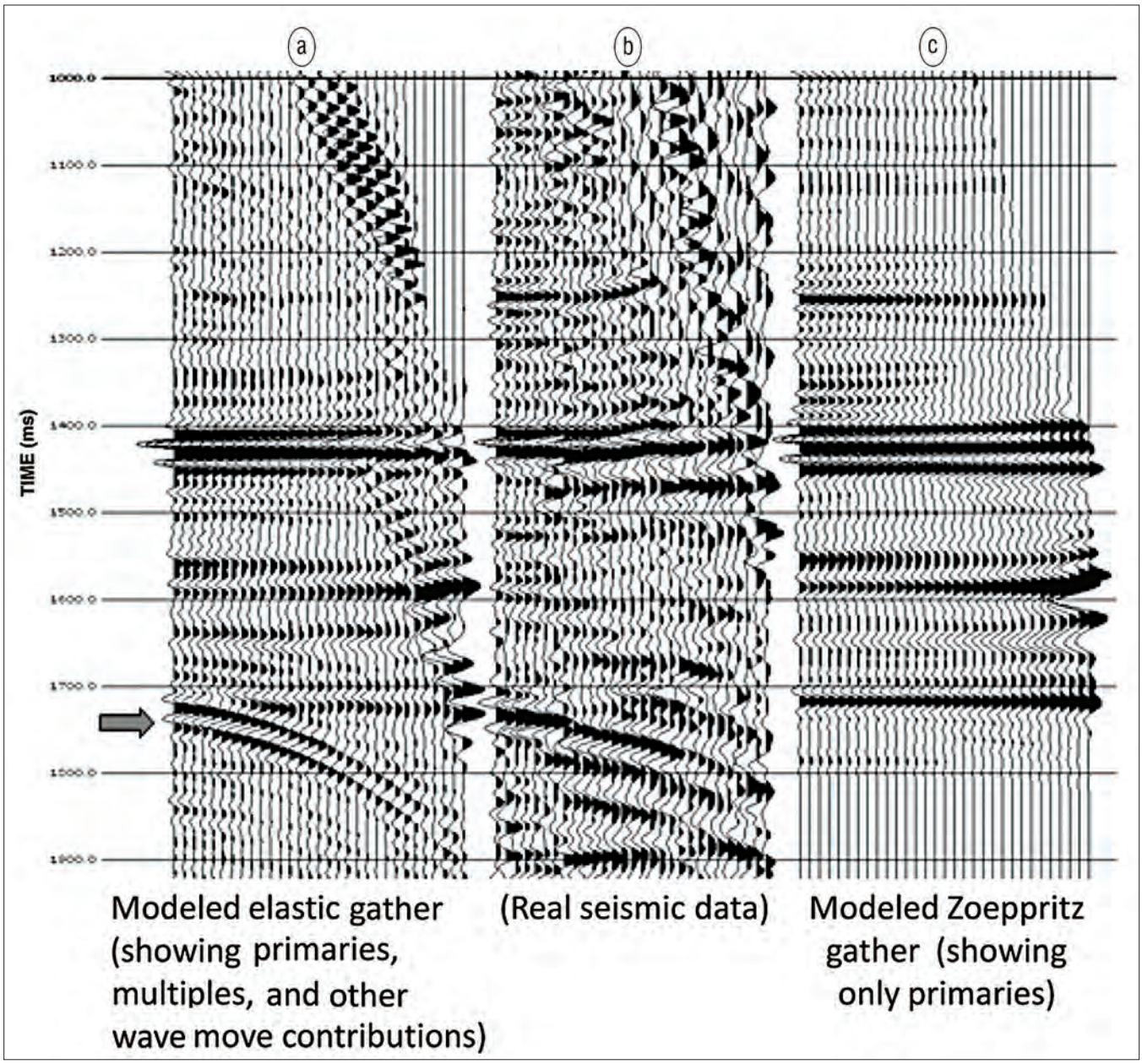

Figure 5. *(a) A modeled elastic gather, (b) the real seismic gather and (c) the modeled Zoeppritz gather. The Zoeppritz modeled gather depicts only the primary events while the modeled elastic gather depicts the primaries including multiples, converted waves, etc. A comparison of these two types of modeled gathers can be used to identify multiples (seen on the elastic gather and absent on the Zoepprtiz gather as shown with the grey arrow). The multiple is seen on the real seismic gather as well.*

the success of bright spots to more subtle anomalies lead to further "amplitude friendly" processing and display workflows.

Complex trace attributes. The efficient fast Fourier transform (FFT) made the computation of "complex trace attributes" almost interactive. Reflection strength, phase, and frequency responses computed using "instantaneous" attributes provided quantitative spectral measurements of the time-varying seismic response that previously had been computed for the trace as a whole. When combined with the new color-display technology, the instantaneous envelope (also called reflection strength) highlighted bright spots and other amplitude variations caused by thin-bed tuning and major lithologic changes. Instantaneous phase attributes highlighted pinch outs, angular unconformities and faults. Instantaneous frequency displays would in some cases show a shift toward lower frequencies below gas sands and oil reservoirs. Coupled with the recently adopted seismic stratigraphy framework, interpreters more rapidly defined depositional environments and extracted attributes favorable for the location of hydrocarbons.

Horizon and formation (interval) attributes. The generation of time-structure maps was and remains one of the key products of any seismic interpretation. Horizon attributes

such as dip magnitude, dip azimuth, and amplitude extractions (Daley et al., 1989) as well as attributes computed from an interval about a picked horizon or between two picked horizons (Sonneland et al., 1989) were introduced in the mid-1980s. By aligning subtle variations (such as small changes in dip indicating a fault) such attribute maps highlighted details that were otherwise overlooked on vertical seismic sections. Dip-magnitude and dip-azimuth maps provided interpreters a means to relate variation in horizon characteristics to paleogeographic elements (Brown and Robertson, 1985), while amplitude extractions of seismic horizons revealed features directly related to lithology, porosity, and the presence of gas. The rms amplitude and other statistical measurements made over an analysis window or between two picked horizons highlighted features such as stacked channels that fell between pickable horizons.

Coherence. By the 1990s, 3D seismic surveys were being used on a routine basis by oil and gas companies. Volumetric calculations of instantaneous attributes, rms amplitude, average absolute amplitude and other single-trace attributes were used routinely to quickly identify anomalies. Looking for an attribute that correlated across multiple surveys with different amplitude, phase, and frequency characteristics, Mike Bahorich recalled the coherence (normalized crosscorrelation) work used in the CoCorp deep crustal imaging effort. The resulting seismic coherence attribute applied by Bahorich and Farmer (1995) to 3D seismic surveys took the industry by storm. Since that time, coherence and coherence-like calculations have been generalized to include semblance (Marfurt et al., 1998), Sobel filters, (Luo et al., 1995), eigen-decomposition (Gersztenkorn and Marfurt, 1999), and energy-ratio (Chopra and Marfurt, 2008) algorithms which provide increased delineation of stratigraphic and structural edges on 3D seismic volumes. Figure 2 compares a time slice from a seismic volume and its equivalent coherence slice (generated using an energy-ratio algorithm). Note the subtle channel definition on the coherence image is not obvious on the seismic amplitude image.

Curvature. Murray (1964) computed curvature of surfaces computed from well bores and correlated anomalous strain to fractures in the Bakken Formation. Roberts (2001) extended this workflow to horizons computed from 3D seismic data. Bergbauer et al. (2003) showed the value of analyzing such curvature images at different scales, which was then extended to volumetric computations by Al-Dossary and Marfurt (2006). Such volumetric curvature attributes provide valuable information on fracture intensity and orientation in zones where horizons cannot be easily picked. Coherence and curvature attributes are commonly used together for mapping structure and depositional sequences. Both these attributes are a great aid in the interpretation of fault and fracture lineaments, generating rose diagrams, and calibrating proximity of anomalies to natural and induced fractures seen in image logs to develop a more quantitative interpretation. Figure 3

compares chair displays where the vertical section is from the seismic volume and the horizon slices are from the coherence and curvature volumes. The curvature volumes are computed using both long-wavelength and short-wavelength operators (Chopra and Marfurt, 2007). Note how the long-wavelength curvature delineates broad anticlines and synclines within the fault blocks whereas the coherence and short-wavelength curvature are more tightly correlated to the faults.

Structural curvature, such as shown in Figure 3, is a lateral second-order derivative of the structural component of seismic time or depth of reflection events. A more recent development is the application of lateral second-order amplitude, energy, or acoustic impedance derivatives along the reflections (Chopra and Marfurt, 2011) which (because the arithmetic is so similar to structural curvature) is referred to as amplitude curvature. For volumetric structural curvature, we compute first-derivatives of the volumetric inline and crossline components of structural dip. For amplitude curvature, we apply a similar computation to the volumetric inline and crossline components of the energy-weighted amplitude gradients, which represent the directional measures of amplitude variability. Because the amplitude and structural position of a reflection are mathematically independent properties, application of amplitude curvature computation to real seismic data often shows different, and sometimes more detailed illumination of geologic features than structural curvature. However, many features, such as the delineation of a fault where we encounter both a vertical shift in reflector position and a lateral change in amplitude, will be imaged by both attributes, with images "coupled" through the underlying geology.

A comparison of structural and amplitude curvature computed for the same seismic survey often shows a higher level of lineament detail or definition of features seen on both long- and short-wavelength amplitude curvature in preference to structural curvature. Such fine detail is useful when using curvature attributes for fault/fracture delineation, particularly those that give rise to measurable amplitude changes but minimal changes in dip, such as cleats in coal beds and diagenetic alteration of fractures in carbonates.

Reflector rotation and reflector convergence. Mathematically, curvature is based on second derivatives of quadratic surfaces. Not all geologic surfaces are quadratic, with rotation about faults being an obvious example. Rotation is a vector with the more natural components being the component perpendicular to the average reflection normal and the orthogonal components parallel to the average reflection normal (Marfurt and Rich, 2010).

We illustrate the reflection convergence and rotation about the normal attributes on a 3D seismic volume from Alberta, Canada. The reflection convergence attribute gives the magnitude and direction of thickening and thinning of reflections on uninterpreted seismic volumes. Reflection rotation about faults is clearly evident and has a valuable application in mapping of wrench faults and subtle rotation about simpler normal and reverse faults. Such attributes would yield convincing results on good quality data sets. Figure 4a shows a time slice at t = 1.330 s from the reflector rotation about the average reflection normal attribute. The yellow arrow is

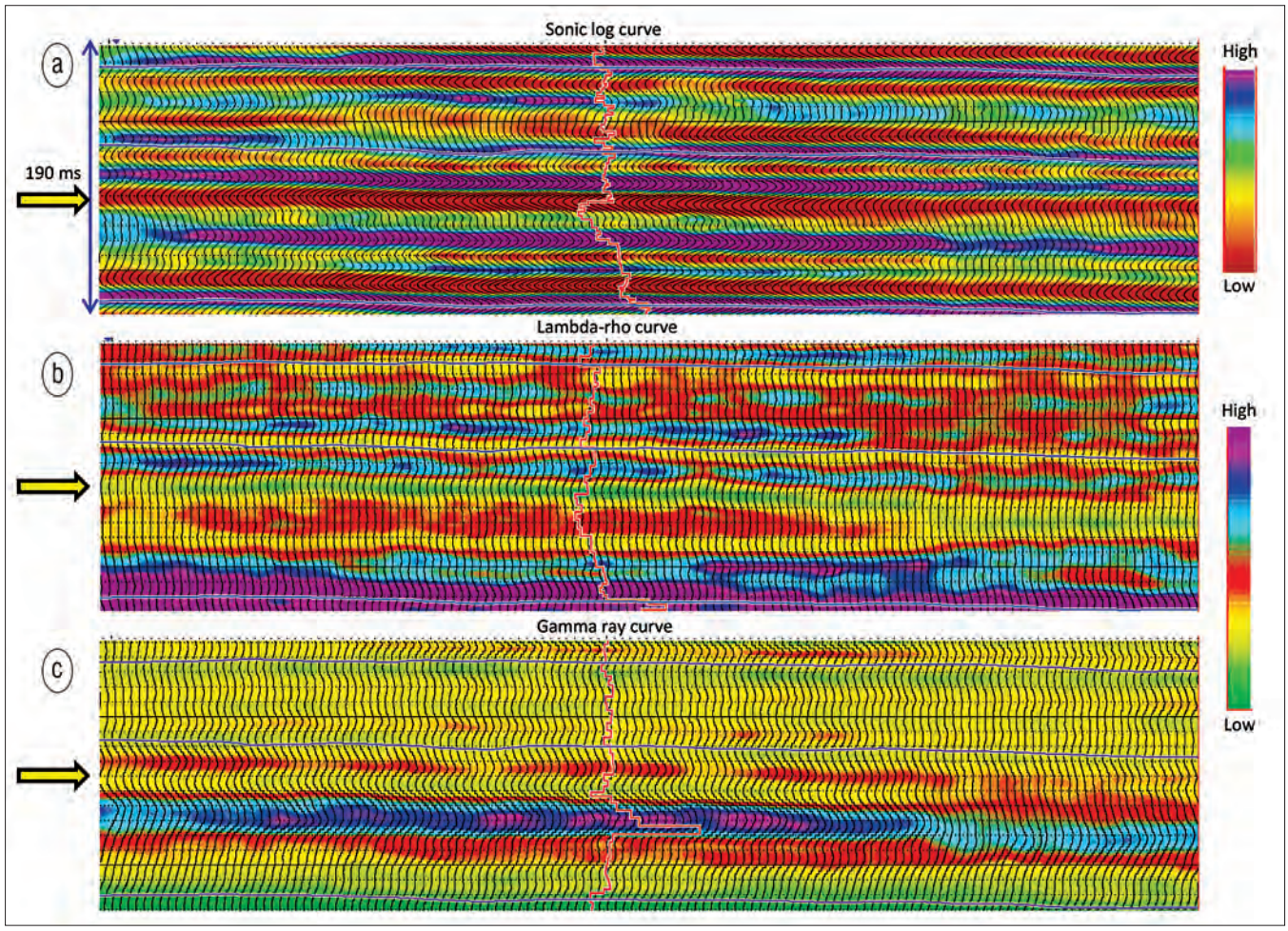

Figure 6. *Segment of a seismic section from (a) P-reflectivity with the sonic log curve overlaid, (b) derived lambda-rho attribute with lambda-rho log curve overlaid, and (c) the derived gamma-ray attribute using extended elastic impedance with the gamma-ray log curve overlaid. The yellow arrows indicate a somewhat shaley sandstone zone which is gas impregnated. Notice the zone exhibits low values of lambda-rho as expected and somewhat lower values of gamma-ray as well. (Data courtesy of Athabasca Oil Sands).*

indicative of either a rotation about antithetic faults or a suite of relay ramps. Figure 4b shows an equivalent time slice from the reflection convergence attribute volume. The display uses a 2D color wheel; blue indicates reflections pinching out to the north, red to the southeast and cyan to the northwest. Figure 4c corenders these two attribute time slices. The thickening and thinning of the reflection appear to be controlled by rotating fault blocks.

Spectral decomposition. Although time-frequency analysis had been used by geophysicists for some time, Partyka et al. (1999) introduced spectral decomposition as an interpretation tool that decomposed seismic data into discrete frequency volumes within the seismic frequency bandwidth. Besides providing a powerful seismic geomorphology tool, spectral decomposition is commonly used to estimate bed thickness (Marfurt and Kirlin, 2001) and as a direct hydrocarbon indicator (Castagna et al., 2003).

Interpretation and rock properties

Rock properties systematic. Understanding how seismic amplitudes change with reservoir lithology, porosity, and fluid product requires a deep understanding of the underlying rock physics. Usually, at the location of a drilled well, we have measurements that give us a good idea of the elastic and physical properties of the subsurface (velocity, density, lithology, porosity, confining stress, pore pressure, saturation, fracturing, etc.). Rock physics systematics provides a means to predict the seismic amplitude behavior away from well control, in areas we may hypothesize to be favorable for additional hydrocarbon accumulation.

In 1982 many oil companies had their own rock physics laboratories. Because of the longer-range objectives and the need to assemble large databases, today such laboratories are found primarily within five or six universities and a few service companies. The focus of rock physics analysis started with estimating porosity and permeability of sandstones and carbonates. Today, much of the research is focused on unconventional reservoirs and on estimating rock strength or "frackability" and the presence of total organic carbon.

Crossplotting. For quantitative AVO interpretation, one needs to know how compressional velocity, V_P, shear velocity, V_S, and density are related to rock properties such as

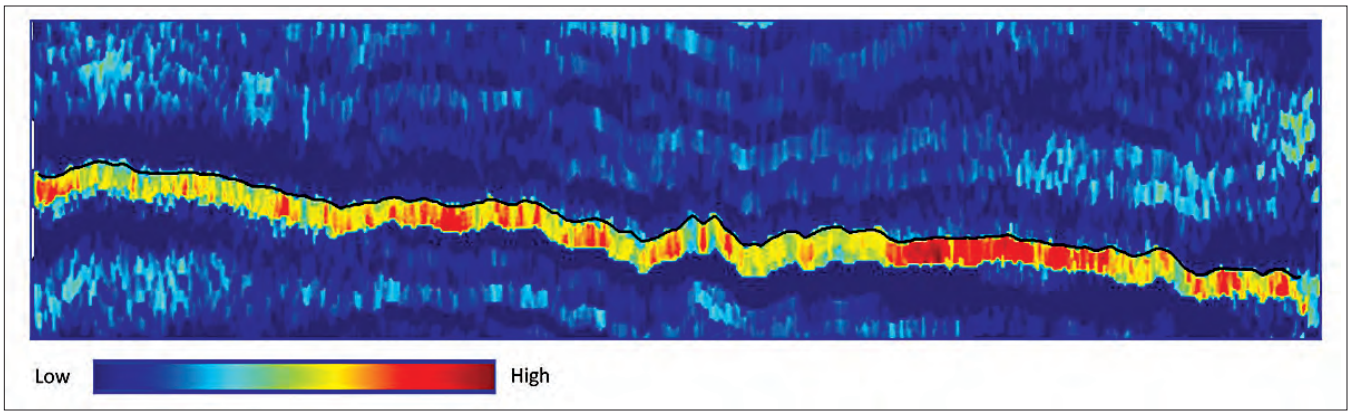

Figure 7. *Segment of a profile from the relative acoustic impedance run on thin-bed reflectivity volume. Notice the lateral variation in impedance seen in the carbonate reservoir zone seen in hot colors as compared with the lower impedance values above and below (from Todorovic et al., 2011).*

lithology, porosity, and fluid content (Castagna et al., 1993). The relationship between velocity and density (or porosity) is not straightforward and is often a function of effective pressure, pore structure and degree of lithification. Consequently, these relationships are not tightly constrained by theoretical composite medium modeling and empiricism is generally relied upon to describe these dependencies (Wyllie et al., 1956; Gardner et al., 1974; Raymer et al., 1980, Han et al., 1986, Goldberg and Gurevich, 1998; Mavko et al., 2003). Typically, lithologic properties such as porosity or frackability are estimated using a full suite of well logs and core measurements. Ideally, rocks having a color-coded property value of interest (high porosity, brittleness) will "break out" and form a cluster when plotted against parameters measured from surface seismic (e.g., AVO slope and intercept or prestack inversion values of $\lambda\rho$ and $\mu\rho$).

Forward modeling. Forward seismic modeling is a key tool in calibrating seismic processing and imaging workflows. Interpreters use forward modeling to achieve a computationally simpler, but no less-important objective. The simplest form of seismic modeling is the generation of synthetic seismograms from well logs and their subsequent comparison with poststack seismic data. More sophisticated, prestack forward modeling of migrated seismic gathers provides the prediction of whether a given hypothesized rock property (cluster in a crossplot) can be separated from the background from surface amplitude measurements. Figure 5 compares a wave-equation elastic modeled gather, a measured seismic gather, and a Zoeppritz gather. The Zoeppritz gather shows only the primary events, while the wave-equation elastic gather shows the primaries, with multiples, and converted waves as well. The grey arrow indicates a multiple, which is seen on the modeled and the real gathers but not on the Zoeppritz gather.

Ideally, forward modeling should take place before undertaking expensive acquisition and sophisticated processing. If forward modeling of the rock physics of the reservoir and seal do not support a measurable anomaly at the surface, an expensive program of time-lapse seismic acquisition and monitoring may be fruitless. In contrast, if forward modeling indicates that a measurable azimuthal anisotropy anomaly can be detected at the surface, a wide-azimuth survey followed by vector-tile migration may well be justified.

Poststack impedance inversion. Poststack, or "acoustic" impedance inversion is the inverse of poststack forward modeling. As stated earlier, impedance inversion was introduced in the mid-1970s by Lavergne (1975) and Lindseth (1976, 1979) and quickly became popular because of the ease and accuracy of interpretation of impedance data in terms of lateral change in lithology and porosity. Simple recursive inversion provided a band-limited estimate of acoustic impedance. Early estimates of "absolute" or broad-band estimates of acoustic impedance were generated by augmenting these estimates with the low-frequency impedance trend measured at and interpolated between well locations. These early efforts were revisited in the mid-1980s with mathematically more rigorous model-based inversion.

Model-based inversion is perhaps the most-widely used impedance inversion method. The interpreter integrates well control and horizon picks to generate (usually through kriging) a low-frequency background model. A synthetic trace is generated from the model and compared with the equivalent seismic trace. The difference between the two is minimized by iteratively perturbing the model in terms of reflection time and impedance which ultimately yields lateral and temporal impedance changes. The original implementations found a solution near the original background model (called a local minimum) by linearizing the equations about the background model and solving using a constrained least-squares technique. Since the late 1990s, these local solution techniques have been augmented with simulated annealing and/or genetic algorithms that find the best (or global minimum) solution.

Given the band-limited nature of seismic data, inversion solutions are nonunique. Classical inversion techniques often favor the "smoothest" impedance model that fits the data. In contrast, the constrained sparse-spike inversion workflow favors "blocky" models represented by a finite number of discrete reflections, or spike. Early implementations were similar to the maximum likelihood deconvolution approach (Chi et al., 1983, 1984; Kormylo and Mendel, 1983) while others

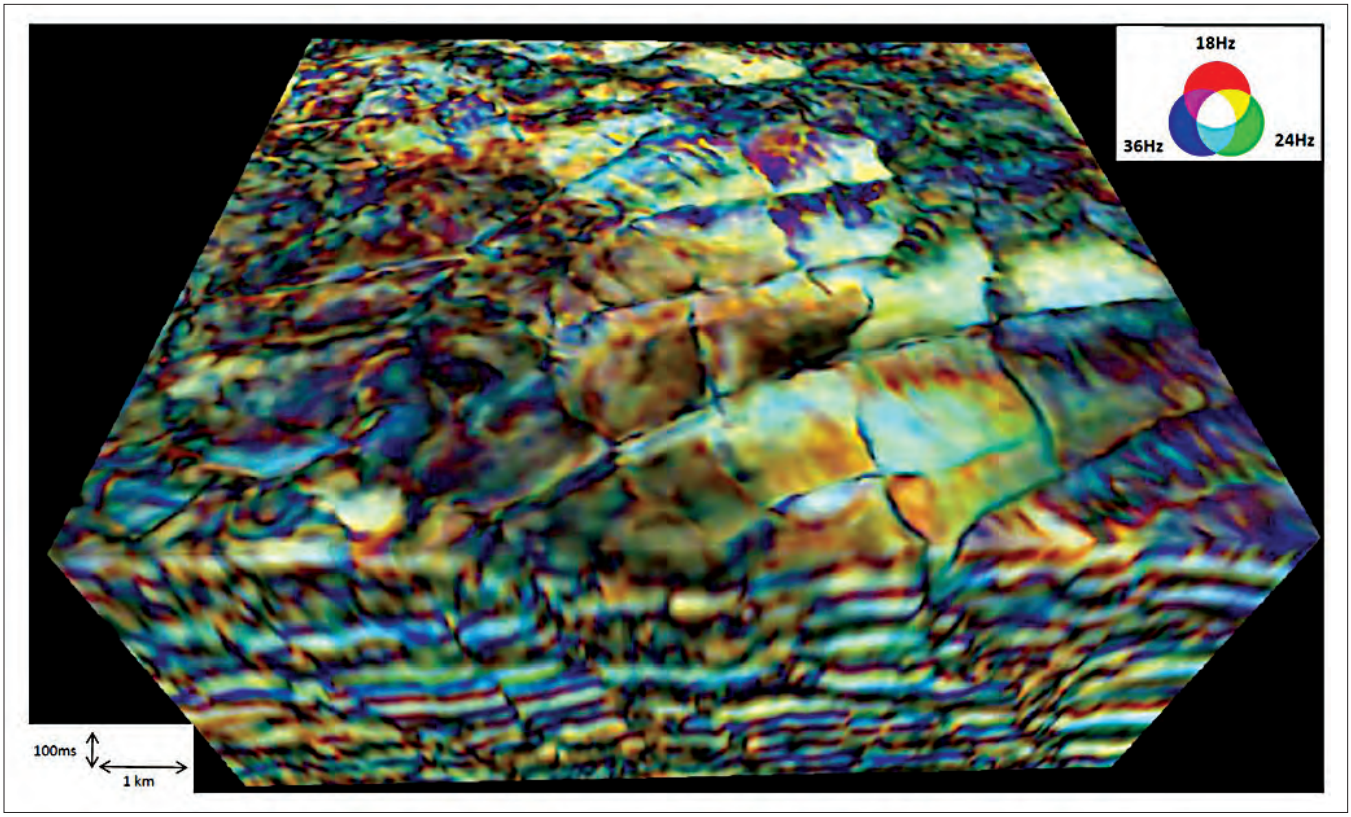

Figure 8. *Volume RGB blend of 18 Hz, 24 Hz, and 36 Hz magnitude responses. Red represents areas where the 18 Hz is dominant, green represents areas where the 24 Hz is dominant, and blue represents areas where the 36 Hz is dominant. Faults are clearly seen as dark black lineaments resulting from a low response from all three magnitudes (modified from Purves and Basford, 2011).*

used an L^1 norm (least-absolute-value rather than the L^2 least-squares) criterion (Oldenburg et al., 1993). These spikes are then transformed into impedance. Sparse-spike impedance inversion exhibits higher resolution and is favored when the blocky assumption fits the geology.

Stochastic (or geostatistical) inversion further expands the seismic bandwidth (Haas and Dubrule, 1994). The interpreter uses the well control to not only build a low-frequency background model, but also to construct a high-frequency (e.g., ½-foot resolution) vertical variogram. The lateral variogram is built from the seismic amplitude data. Because the model extends well beyond the limits of seismic resolution, many models that fit the variogram also fit the seismic amplitude data. For this reason, a suite of as many as 100 or more realizations is generated. In principle, the average impedance of these realizations is the same as the model obtained from classical model-driven inversion. In practice, the interpreter sorts the realizations by a parameter of interest (such as total pore volume for impedance values below a given threshold) and generates P_{10}, P_{50}, and P_{90} models to be used in subsequent risk analysis.

Elastic impedance inversion of angle-limited stacks. Given a poor zero-offset stack with residual multiples, Connolly (1999) introduced the concept of "elastic impedance" which is the result of inverting an angle-limited stack. Analysis of the Aki-Richards approximation to the Zoeppritz equations shows that elastic impedance is a product of density, P-impedance, and S-impedance whose exponents depend on the angle of incidence and background V_S/V_P ratio. Often, a mid- to far-angle stack is more sensitive to fluid content than the near-angle stack such that elastic impedance may be more useful than acoustic impedance. An additional advantage of elastic impedance is that a wavelet is estimated for each stack, removing much of the shift to lower frequencies generally seen on far traces.

Amplitude variation with offset (AVO) analysis. Examination of prestack amplitude gathers often shows a variation with offset (and hence with incident angle). With the common use of relative amplitude processing for bright spot analysis, early theoretical work on amplitude changes with incident angle due to lithology changes could be put into practical use. The first use (Rutherford and Williams, 1989) was to further the identification of gas sands in Tertiary basins (which give rise to what we now call class III AVO anomalies). It was realized soon that processing and acquisition effects could lead to interpretation of false AVO anomalies and that such effects need to be considered carefully. In the mid-1980s, shear-wave velocity log measurements were not routinely made but rather were often estimated with simple empirical relationships, leading to inaccurate AVO predictions. Since the 1980s, the introduction of 3D seismic surveys, careful processing of the data in terms of "true-amplitude" processing, the use of full-waveform sonic logs, enhanced rock property systematics, and careful seismic modeling have all contributed to bring-

ing AVO technology to the seismic interpreter. Needless to mention, an important role was played by commercial software packages (such as that by Hampson and Russell) that put this technology on the interpreter's workstation.

Velocity versus azimuth (VVAz) and amplitude versus azimuth (AVAz) analyses. With the introduction of wide-azimuth surveys, both velocity versus azimuth (VVAz) and amplitude versus azimuth (AVAz) have been used to estimate the orientation and spatial variation of naturally-occurring fractures in reservoirs (Gray and Head, 2000; Williams and Jenner, 2002; and Jenner, 2002). VVAz is usually achieved in the processing shop, whereas AVAz can be done by the interpreter using commercial software on a workstation. In this latter workflow, the interpreter first flattens (registers) the far-offset stack of common-azimuth migrated volumes onto a reference pick and then fits the amplitude changes with a curve that varies as $B_{aniso}\cos(2\phi + \psi)$, where B_{aniso} is an estimate of the intensity of anisotropy and ψ is the strike of maximum amplitude from north. Today, VVAz and AVAz are particularly useful in estimating the direction of maximum horizontal stress in order to optimally orient a horizontal well and predict the behavior of a frack job.

Prestack impedance inversion. Prestack impedance inversion is much like AVO analysis, except that a wavelet is derived for each input angle. Extended elastic impedance (Whitcombe et al., 2001) uses seismic modeling to determine which angle-limited stack best correlates to a desired rock property such as bulk and or shear modulus, Poisson's ratio, gamma-ray and water saturation. These parameters are indicative of different lithologies and yield information on fluid fill. Figure 6a shows a segment of a P-reflectivity section and its equivalent sections from the $\lambda\rho$ volume (Figure 6b) and the derived gamma-ray attribute using extended elastic impedance. Notice the gain of information in terms of lower $\lambda\rho$ and somewhat lower values of gamma-ray indicating the shaley sandstone at the level indicated by yellow arrows.

The separately inverted angle-limited stacks can be combined in an AVO-like analysis to create a sequential prestack inversion workflow (e.g., Espersen et al., 2000). Alternatively, the AVO equations can be manipulated to estimate reflectivity components sensitive to P-wave and S-wave impedances. These two components can then be inverted jointly to obtain the P-wave and S-wave impedances themselves. For good quality data, one can attempt to model (and thereby invert) the migrated CMP gather traces simultaneously, and directly obtain P-wave and S-wave impedances. The choice of inversion strategy is strongly dependent on the quality of the input data gathers. In the different inversion methods referred to earlier, the low-frequency component is required to obtain absolute impedance values. If this low-frequency a priori model is known with sufficient accuracy or is close to the true model, such inversion methods could yield accurate results. However, in most cases it is derived from the well logs or estimated from the seismic velocity field and so could be far from the true model. In such cases, these inversion results could be compromised. In prestack waveform inversion, both the low- and the high-frequency components of the P-wave acoustic impedance are extracted from the seismic data (Mallick and Ng, 1995; Mallick, 1989). When the full elastic Earth model is used, in addition to the P-wave acoustic impedance, S-wave information or Poisson's ratio can also be estimated from prestack data. This provides the fluid information for the reservoirs and thus prestack waveform inversion has an advantage over other inversion methods. Prestack inversion is a computationally intensive process as it calculates several synthetic models in its search for the most optimum model at a given CMP location (Mallick, 2001). Most implementations try and reduce the compute time by providing bounds on the search intervals in model space as well as the fineness

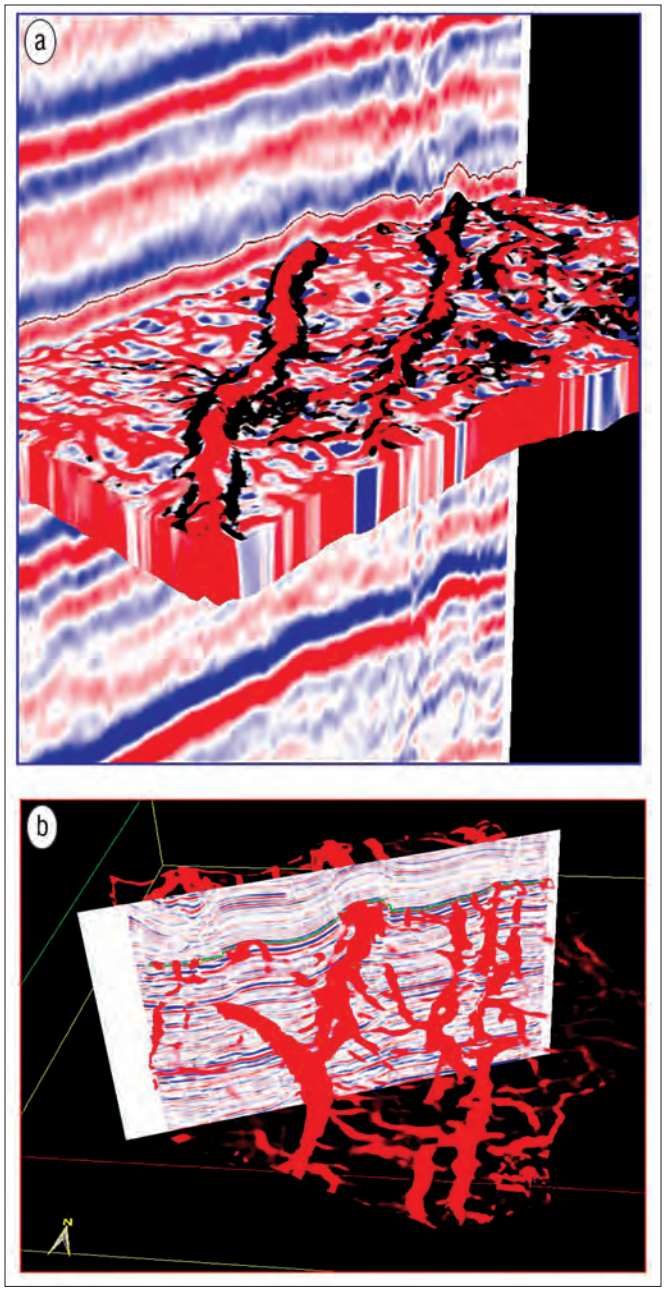

Figure 9. *(a) Strat-cube from the most-positive curvature attribute corendered with coherence seen here in a 3D chair view. (b) Multiattribute display using blending/transparency/opacity.*

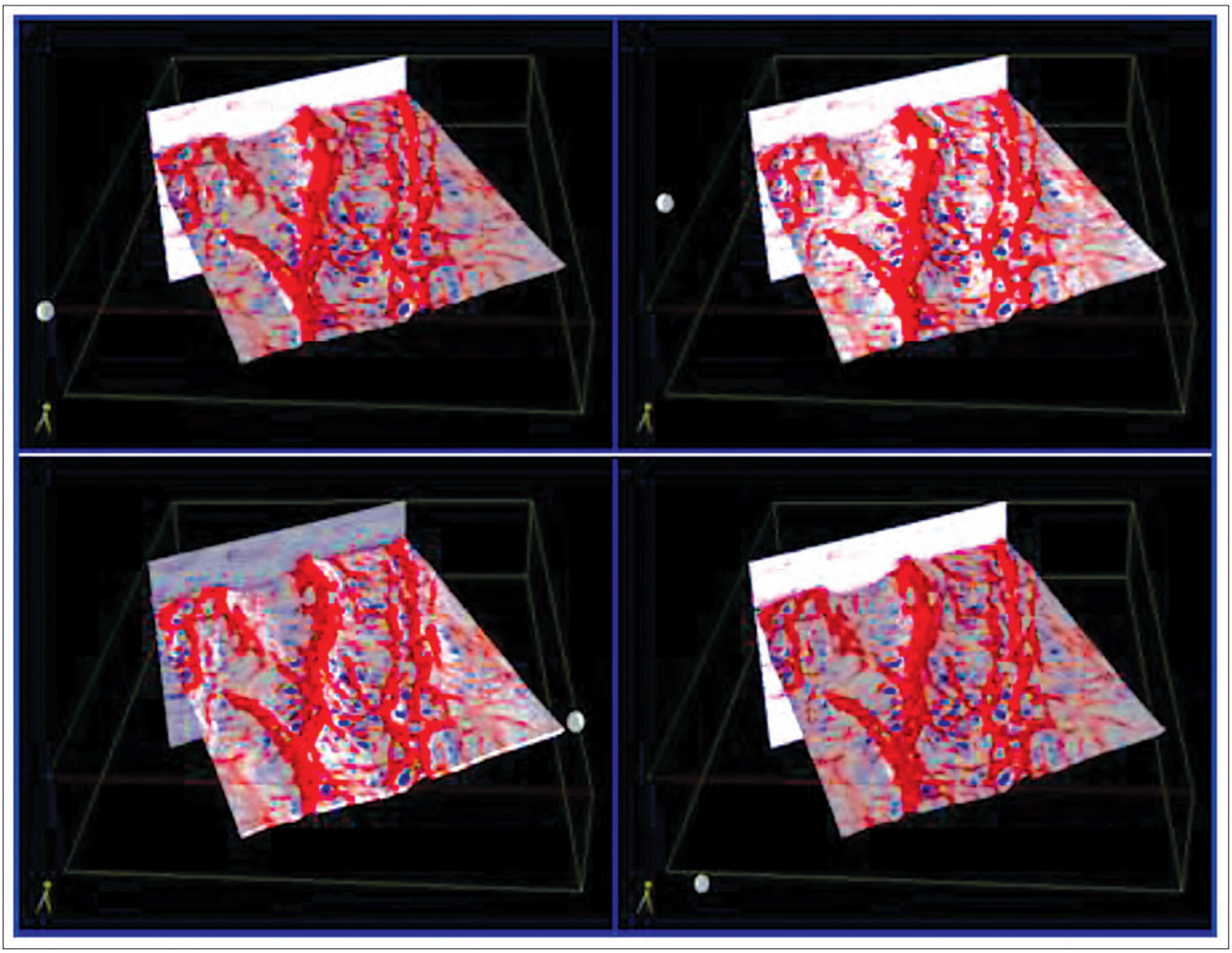

Figure 10. *3D chair view display with the strat cube from the most-positive curvature attribute The light source shown in each image indicates the direction from which illumination takes place. Notice that the movement of the source about the chair display illuminates the faults/fractures better when orthogonal to their strike. Subtle features are seen on the display with other locations of the source.*

with which the model is discretized. However, even with the fastest computers it is difficult to apply prestack inversion to large 3D volumes as production runs. A practical compromise has been reached by devising hybrid inversion, where prestack inversion is run at a selected number of points and the elastic model parameters so generated can be used to constrain the low-frequency model required for poststack inversion (Mallick, 2001).

Data conditioning. Seismic data are usually contaminated with both random and coherent noise, even when the data have been properly migrated and are multiple-free. Seismic attributes are particularly effective at extracting subtle features from relatively noise-free data. Certain types of noise can be addressed by the interpreter through careful structure-oriented filtering or postmigration footprint suppression.

Some kinds of noise such as multiple contamination or severe prestack migration noise require more complete reprocessing. Interpolation has become important in reducing migration noise from irregularly sampled data (Trad, 2009), and was shown by Hunt et al. (2010b) to be crucial for elastic studies.

Another common problem with seismic data is their relatively narrow bandwidth. Significant efforts are made during processing to enhance the frequency content of the data as much as possible to provide a spectral response that is consistent with the acquisition parameters. Ironically, interpreters can be somewhat more aggressive in their filtering. They will have a better understanding of the play concept, access to any well data, and therefore be better able to keep or reject alternative filter products that are consistent or inconsistent with the interpretation hypothesis.

Interpreters use different methods for frequency enhancement for various objectives. One of them is thin-bed reflectivity inversion—a form of spectral inversion which produces sparse reflectivity estimates. It resolves thin layers below the tuning thickness under favorable circumstances when the assumptions are met in practice. Application of thin-bed reflectivity inversion to seismic data can provide significant detail. The interpreter needs to use all such "bandwidth extension" techniques with caution, and carefully compare high-resolution predictions to the high-resolution well control to make sure that the assumptions made in the method are supported

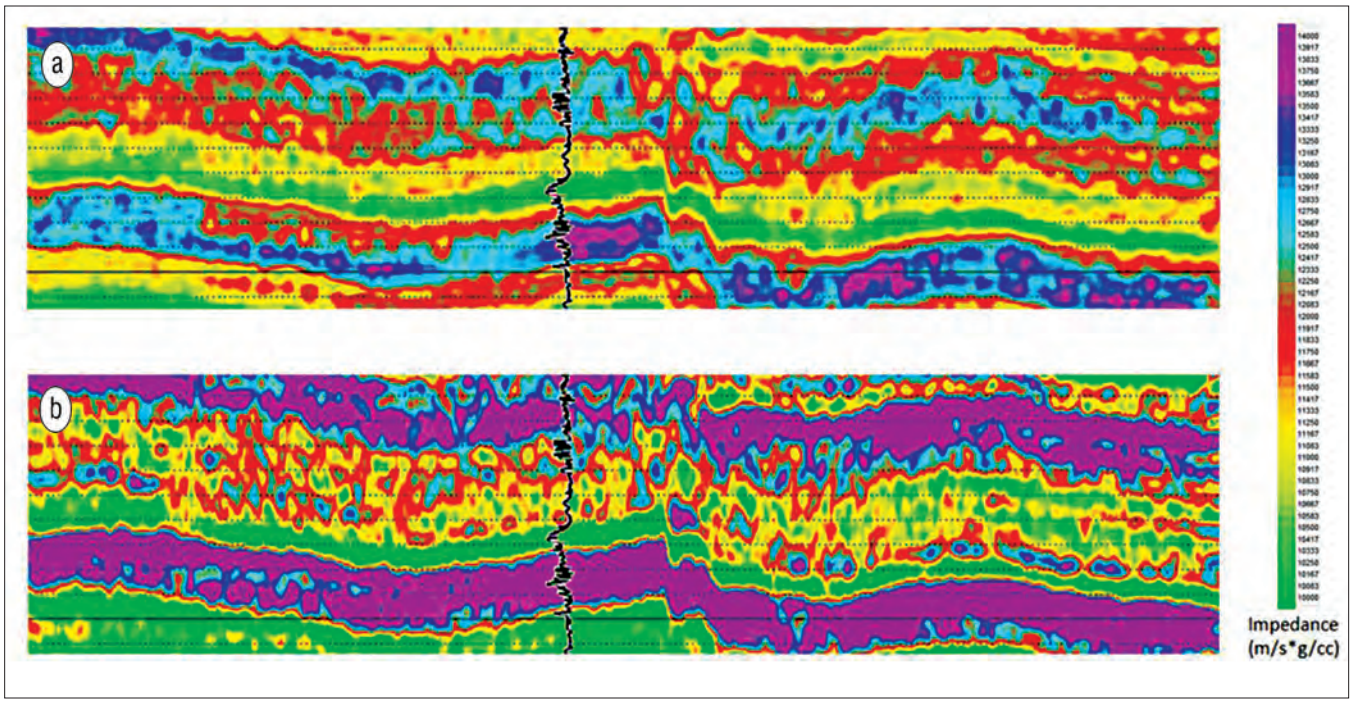

Figure 11. *(a) P-impedance estimated with probabilistic neural network, and (b) P-impedance obtained from poststack inversion. The inserted black curve is the P-impedance log. Notice the higher subtle detail on the neural network inversion and better correlation with the log curve (from Misra and Chopra, 2011).*

by the geology. Figure 7 shows a vertical slice through a relative acoustic impedance volume computed using a thin-bed reflectivity inversion algorithm. The lateral variation in impedance seen in the carbonate reservoir is seen clearly in terms of the hot and cold colors.

Interpretation and data integration

Visualization: color blending, color modulation, and opacity. Visualization is by far the easiest and most commonly used method to integrate data of different types. Early 3D interpretation was a simple extension of 2D interpretation workflows and consisted of interpreting a grid of inlines and crosslines from a 3D seismic volume, autopicking or interpolating intermediate traces, and generating a time-structure map. While such maps are in general superior to those generated from 2D seismic data, little of the seismic information will have been used. Early 3D visualization systems introduced in the 1990s were relatively slow, expensive, and required a significant change in the interpreter's mindset. Today, 3D visualization has undergone a generational change. Not only has the hardware cost been driven down by the computer gaming industry, but the 14-year olds who played those mind-numbing games are now our younger interpreters. Today's interpretation workflows go far beyond traditional time-structure maps and include optical stack based on transparency, multiattribute corendering, multiattribute crossplotting, and geobody detection that provide new insight into prospects and new means of communicating such insights to coworkers, management, partners, and investors.

Today, all workstations provide at least 8-bit (256 colors) color displays. While these are adequate to display data stored as 8-bit integers, corendering and crossplotting of multiple attributes such as spectral magnitude components greatly benefit by greater color depth. Computer terminals (and digital projectors) form color images through the addition of red, green, and blue (RGB) components. Using the OpenGL programming standard, it is fairly easy to corender or blend three images of the same type—such as near-, mid-, and far-amplitudes or low- mid- and high-frequency spectral components (Figure 8). Today, the more recently written interpretation software (such as that used to generate Figure 8) uses 24-bit color, with those companies having a large investment in legacy software working hard to upgrade.

Although not every system has 24-bit color, almost all commercial software provides corendering of two attribute volumes using opacity. Given two attributes, ideally one that is sensitive to amplitude or thickness plotted against hue, and another that is sensitive to edges plotted against a gray scale (Barnes, 2011), a weighted-average of the RGB components can be constructed, giving rise (for say a 50% weight applied to the RGB components of the edge attribute) to a relatively more pastel image of the original amplitude with readily apparent edges delineating lithologies and fault blocks. By setting zones above and below interpreted horizons to be completely transparent, the interpreter can sculpt a subvolume of the 3D seismic data, thereby facilitating the understanding of the spatial disposition of the features of interest. Figure 9a shows a strat-cube from the most-positive principal curvature attribute corendered with coherence cut by a vertical slice through the seismic amplitude volume. Figure 9b shows the strat-slice where transparency is used to display only the high positive curvature values.

Figure 12. *The combined result of interpreting the structure and the depositional systems. The 3D boundaries of the channels were interpreted in the stratal volume, and then inverse transformed back to the structural domain—putting all of the structural effects back in the interpreted channel boundaries so they are properly located in the original seismic data. Inverse transformed channels are shown between the top and bottom horizons of the five horizons used to define the transform (from Dorn, 2011).*

Other types of voxel processing have also rapidly advanced. Rijks and Jauffred (1991) showed how directional illumination (or shaded illumination) of interpreted horizons was a powerful means of enhancing subtle fault edges that fall near the limits of seismic resolution. The angle at which a given display is illuminated serves to help visualize the data clearly and leads to a better understanding of the data being interpreted. Figure 10 shows a chair view of a seismic inline from a 3D seismic volume and a strat-cube from k_1 principal positive curvature. The location of the light source around this image illuminates the discontinuities or the lineaments on the curvature strat slices and so helps visualize the attribute better.

Integrating modern subsurface measurements—image logs and microseismic data. Although geologic models and outcrop analogs (e.g., Hennings et al., 2000) predict the orientation and relative intensity of fractures to folding and lateral stress variations, Hunt et al. (2010) were able to quantitatively demonstrate this correlation between AVAz and curvature attributes with horizontal image logs and microseismic data. Because fractures are a function of strain, lithology, and bed thickness, correlations with a single attribute sensitive to only one of these components (curvature to strain) will not provide optimal correlation. For this reason, multilinear regression using AVAz and curvature can provide a better correlation. Jianming et al. (2009) combined coherence, curvature, VVAz, and shear-wave splitting to form a risk-based prediction of natural fractures measured by image logs in Sichuan Basin, China. Working in an unconventional shale reservoirs, Thompsen et al. (2011) correlated the location of microseismic events to curvature and VVAz attributes and curvature while Refunjol et al. (2011) correlated microseismic events to curvature and $\lambda\rho$-$\mu\rho$ inversion volumes. Dereshowitz et al. (2010) used discrete fracture network (DFN) models to specify parameters such as fracture length, azimuth and intensity with the small-scale fracture measurements from core and image log data, and large-scale measurements from outcrops and 3D seismic attributes, which add spatial variability to the DFN model (Reine and Dunphy, 2011).

Tracking steam fronts in heavy oil reservoirs. The distribution of bitumen in the McMurray Formation in the Athabasca oil sands area of western Canada varies because of high

degree of facies heterogeneity throughout the deposit. This lithological heterogeneity makes it difficult to interpret geology and estimate bitumen distribution. Besides, because of low viscosity (8 API), special production methods are used for extracting the oil. Steam-assisted gravity drainage (SAGD) is one such technique which uses two horizontal wells vertically separated by about 5 m. The upper well injects steam and creates a high-temperature steam chamber around it. This lowers the viscosity of the bitumen which tends to drain through the formation more freely under the action of gravity and is collected by the other horizontal well. SAGD works well in thicker formations where there are no obstructions between the two wells. A change in lithology, the presence of shale stringers in sandstone units, or faults could create problems and reduce the production. As a result the need for formation characterization is paramount.

Two different approaches have been developed for mapping reservoir heterogeneity. One is more suitable when the available seismic data are of good quality and have long offsets. The relationship between reservoir lithology and rock physics parameters needs to be determined, especially in terms of those that can be derived from seismic data, such as P-impedance, S-impedance and density (Xu and Chopra, 2008). The other approach is more appropriate where the drilled wells are somewhat uniformly distributed over the available 3D seismic data. Neural networks are then used with the available log data for training and applied to seismic data for prediction of an appropriate attribute such as gamma ray (Tonn, 2002). Such attempts are promising, technically as well as economically.

Unsupervised classification (clustering). Interpreters routinely cluster alternative seismic measurements (attributes) to better "risk" a given prospect or characterize a reservoir. For example, a target that is structurally high, has four-way closure, and has a class III AVO anomaly is an excellent prospect in most Tertiary basins. The computer literature is rich in alternative clustering strategies. Although k-means and other methods have been used, variations of the Kohonen self-organizing map (SOM) are today the most popular in analyzing geophysical data. The earliest applications considered each of n stratal slice through a seismic amplitude volume to be an attribute. The results of SOM is *m* clusters, each defined by its mean and standard deviation in *n*-dimensional space. Using Baysian classifiers, the windowed data at each survey location are then assigned to the nearest cluster mean. Because the stratal slices are through seismic amplitudes, the *n*-dimensional mean appears as an *n*-dimensional waveform, such that this method is commonly called waveform classification.

In its original implementation, waveform classification was totally unsupervised. Subsequent implementations allowed the interpreter to introduce and modify specific waveforms, such as average waveforms representing good and bad wells (Poupon, 2004). SOM can be applied to any suite of attributes, providing a clustering technique that can be an excellent means of characterizing geomorphology (Strecher and Uden 2002; Coleou et al., 2003; Roy et al., 2011).

Supervised classification and probabilistic neural networks (PNN). The earliest implementation of supervised classification involved cross-correlating the seismic waveform (e.g., Johnson, 2000) or vector of attributes (e.g., Michelena et al., 1998) about one or more wells with the seismic waveforms or vector of attributes extracted about an interpreted surface. Seismic locations with high correlations were judged to have a similar behavior to that at a given well.

Probabilistic neural networks provide a numerical framework for doing such correlations where there are multiple discrete facies or continuous rock parameters, such as porosity to estimate. To work well, the desired output must have some underlying linear or nonlinear correlation to the attributes used. For the prediction of continuous rock parameters, the mathematics of artificial neural networks (ANN) prediction is not unlike that used in predictive deconvolution. Discrete predictions use a sigmoidal function varying between 0 and 1 in the perceptron, where positive arguments of the sigmoidal function produce a "true", or +1, result and large negative arguments produce a "false", or 0, result. Combined with other perceptrons, each facies will be assigned a true or false value at each voxel.

In facies analysis, the interpreter simply picks locations in the seismic data volume that represent each of the desired facies, including facies that the interpreter is not interested in, but that represent a significant portion of the data volume. Next, the interpreter selects a suite of attributes that characterize and ideally differentiate the seismic facies. The picked event locations are used as training data to derive a nonlinear relationship between the input attribute volumes and output user-defined facies classification (e.g., shale, salt, mass transport complex, sand fan, etc.). Once trained, the ANN predictions are validated using interpreter-defined facies not used in the training step. If this validation is acceptable, then the ANN is applied to the entire data volume and the prediction is used in subsequent analysis. If the validation is unacceptable, additional attributes may need to be added to (or removed from) the analysis to further differentiate the facies. One of the earliest applications of ANN to seismic facies recognition was in the identification of gas chimneys (Mehldahl et al., 1999).

A probabilistic neural network (PNN) approach to impedance inversion could be used where two runs of PNN first produce estimates of P-velocity and density from a uniform distribution of sonic and density log data. In addition to amplitude, other attributes such as amplitude envelope, amplitude and weighted frequency are tested in a multilinear regression framework for optimal selection of attributes which ultimately are used for the inversion. Figure 11 compares the PNN and the conventional model-based inversion on data from a gas play in Alberta, Canada. As expected the impedance section from PNN shows more subtle impedance variation than the model-based inversion because the former is largely driven by well logs. The overlaid impedance log shows a better correlation with events on PNN inversion than the model-based inversion.

Interpretation in the future

We base our prediction of the future from advances made in

the last two or three years. We think that most of the advances will be driven by need rather than by researchers thinking of great ideas. We predict that the next two decades will see a continued progression away from exploration with an ever-increasing focus on frontier resource plays. These plays include coal-bed methane, shale reservoirs, oil sands, and tight sandstone and limestone reservoirs. These plays have limited permeability and require horizontal wells with multistage hydraulic fracturing and/or acidization to be economic. Our work will focus on the equations that define production capability and fracture stimulation. This means we will estimate small changes in permeability as well as the mineralogic changes that affect completion quality. Geoscientists will need to predict "frackability" of shales, "deliverability" of coal seams, permeability-related facies changes in tight reservoirs, wellbore stability in soft sediments, and differentiating between local fractures that enhance production and through-going fractures that connect to underlying or overlying aquifers in carbonate plays.

Integration of new types of subsurface data will be key. Today, microseismic data are commonly used to assess the performance of hydraulic fracturing workflows. Future work will use the same types of measures, correlated with prestack inversion, to identify bypassed pay missed by the first frack job. Work such as that by Hunt et al. (2010) using microseismic and image logs in horizontal wells to map natural and induced fractures in carbonates and correlating them to surface seismic measurements. This kind of effort can be rerun after the first frack job to assess the quality of completion. Production logs will be run to map open fractures, correlating them to surface seismic measurements, and thereby modifying subsequent drilling decisions and skipping of stages to avoid hydraulic fracturing into surrounding aquifers.

Today, it is not uncommon to hear small operators refer to the development of a mature field as a "statistical play" implying that no 3D seismic data are needed. We envision the statistical play of the future to be more like the Wamsutter play of today (Michelena et al., 2011) where seismic data are used not to find the one best location, but also are combined with modern geostatistics and invariant embedding to increase our success of infill wells by 10–20%. In order to correlate productivity measures from long, multistage horizontal wells to seismic data, we will have to find better ways to deal with the issues of support in these different types of data.

Today, most long-offset (those exceeding two times the depth) seismic data are muted out, whether in ocean-bottom seismometry or acquisition over relatively shallow shale gas targets. We will need not only to develop improved elastic processing techniques honoring anisotropic and heterogeneous media, but also to extend our modeling and inversion algorithms and interpretation workflows to estimate anisotropy at the formation and even shallower bed level, providing a means to identify areas of high TOC giving rise to "sweet spots."

Wide-azimuth data are cost-effective in the land environment today, with the only requirement being more recording equipment and higher recording capacity. We expect that with the ever-increasing focus on horizontal drilling in resource plays that wide-azimuth data will become the new standard and subsequent AVAz analysis routine. We predict (pray?) that continued advances in slip-sweep, encoded, single vibrator acquisition will make-high density land seismic data routine in areas that do not have significant access costs, removing the acquisition footprint headache from our workstations and providing enhanced suppression of shallow side-scattered noise (Pramik, 2011).

While the acquisition hardware is here, and most of the processing algorithms in place, the adoption of multicomponent data will be driven by interpreters. Multicomponent data, and converted-wave data in particular, need to be carefully evaluated in terms of their impact on reservoir appraisal and production workflows for field development. Barring significant processing breakthroughs, converted-wave data will provide at best comparable structural images for most reservoirs, and their greater value will be in estimating rock properties. Do multicomponent data provide more accurate estimates of rigidity ($\mu\rho$) and incompressibility ($\lambda\rho$) that can better guide a given completion strategy? Do multicomponent data and shear-wave splitting better delineate induced fractures or map bypassed pay?

The future of interpretation software will also progress rapidly as evidenced by recent advances. Graphical processing units (GPU) or their future successor will become integrated in most commercial interpretation software products, rendering fast, truly interactive interpretation of large, multiattribute data volumes (James et al., 2011). Geobody/object extraction will progress well beyond estimating the probability, strike, and dip of faults. Shrink-wrapping (mathematically, "level set") technology will be deployed to "extract" nonplanar features such as channels, carbonate buildups, and salt domes. 1990 technology of interpreting on "flattened" sections will be replaced by interpretation on palinspastically reconstructed volumes (flattened sections work only for simple layer-cake geology which does not require a more rigorous treatment of palinspastic method) or Wheeler volumes that better represent structural and stratigraphic relationships in paleo time. In Figure 12, we show a combined result of interpreting the structure and the depositional systems.

Many seismic advances of the 1980s and 1990s were facilitated by the rapid advance of computer power. Similar advances in computer gaming technology of the 1990s and 2000s led to widespread adoption of modern 3D visualization technology. Neither of these advances was driven by the seismic industry, which is a relatively small market in the world economy. A major impetus in 2012 is in pattern recognition—with government security and drug enforcement agencies pushing facial recognition and tracking telecommunication activity and private industry identifying and exploiting patterns in e-commerce and Web searches. We cannot predict where these trends will lead, but they too will be adapted to seismic interpretation. In summary, we expect the future of seismic interpretation to offer unprecedented capabilities which will continue to amaze us.

We have here reviewed some history of seismic interpretation, and we have summarized tools and capabilities that

the interpreter has available today. But we could go on. We have not discussed the basic workstation capabilities of tracking and mapping. We have not discussed the ever-present dilemma of distinguishing genuine geologic information from noise. We have not discussed other geophysical techniques outside the seismic realm. We have not discussed geology, an essential ingredient of seismic interpretation, and the majority of seismic interpreters today have degrees in geology. We have not discussed the actual techniques of finding oil and gas. In short the job of seismic interpretation, most commonly directed to finding and producing more hydrocarbon, is a complicated challenge. Are today's geoscientists able to handle the task? Too many users of today's workstations extract an attribute because it exists, not because there is an established or postulated purpose. Too many people who call themselves "interpreters" are bewildered by the technology and are simply looking for magic. We may well find in the future that the greatest limitation to industry progress is people, not the workstation tools, nor the data available. Hence, in order for our industry to move forward, we will need more education and training of geoscientists and the management who direct them. TLE

References

Al-Dossary, S. and K. J. Marfurt, 2006, 3D volumetric multispectral estimates of reflector curvature and rotation: Geophysics, **71**, no. 5, 41–P51, http://dx.doi.org/10.1190/1.2242449.

Allen, J. L., T. Giardinelli, and W. T. Reynolds, 1995, Three Fresnel zone examples: 65th Annual International Meeting, SEG, Expanded Abstracts, 120–123.

Canning, A. and G. H. F. Gardner, 1998, Reducing 3-D acquisiton footprint for 3-D DMO and 3-D prestack migration: Geophysics, **63**, no. 4, 1177–1183, http://dx.doi.org/10.1190/1.1444417.

Bahorich, M. S. and S. L. Farmer, 1995, 3D seismic discontinuity for faults and stratigraphic features: The coherence cube: 65th Annual International Meeting, SEG, Expanded Abstracts, 93–96.

Barnes, A. E., 2011, Displaying seismic data to look like geology: GCSSEPM 31st Annual Bob. F. Perkins Research Conference, 100–119.

Bergbauer, S., T. Mukerji, and P. Hennings, 2003, Improving curvature analyses of deformed horizons using scale-dependent filtering techniques: AAPG Bulletin, 87, no. 8, 1255–1272, http://dx.doi.org/10.1306/0319032001101.

Bodine, J. H., 1984, Waveform analysis with seismic attributes: 54th Annual International Meeting, SEG, Expanded Abstracts, 505–509.

Bodine, J. H., 1986, Waveform analysis with seismic attributes: Oil & Gas Journal, 84, no. 23, 59–63.

Brown, A. R., and J. D. Robertson, 1985, Seismic interpretation for detailed exploration development and production: The Leading Edge, 4, no. 10, 60–65, http://dx.doi.org/10.1190/1.1439107.

Castagna, J. P. and M. M. Backus, 1993, Offset-dependent reflectivity—theory and practice: SEG.

Castagna, J. P., S. Sun, and R. W. Siegfried, 2003, Instantaneous spectral analysis: Detection of low-frequency shadows associated with hydrocarbons: The Leading Edge, **22**, no. 2, 120–127, http://dx.doi.org/10.1190/1.1559038.

Chi, C. Y., J. M. Mendel, and D. Hampson, 1983, A computationally fast approach to maximum-likelihood deconvolution: 53rd Annual International Meeting, SEG, Expanded Abstracts, 359–363.

Chi, C. Y., J. M. Mendel, and D. Hampson, 1983, A computationally fast approach to maximum-likelihood deconvolution: Geophysics, **49**, no. 5, 550–565, http://dx.doi.org/10.1190/1.1441690.

Chopra, S. and K. J. Marfurt, 2007, 3D seismic attributes for prospect generation and reservoir characterization: SEG.

Chopra, S. and K. J. Marfurt, 2008, Gleaning meaningful information from seismic attributes: First Break, **26**, no. 9, 43–53.

Chopra, S. and K. J. Marfurt, 2011, Structural curvature versus amplitude curvature, 81st Annual International Meeting, SEG, Expanded Abstracts, 980–984.

Claerbout, J. F., 1986, Velocity extrapolation by cascaded 15 degree migration: SEP-48, 79–84.

Coleou, T., M. Poupon, and K. Azbel, 2003, Unsupervised seismic facies classification: A review and comparison of techniques and

implementation: The Leading Edge, **22**, no. 10, 942–953, http://dx.doi.org/10.1190/1.1623635.
Connolly, P., 1999, Elastic impedance: The Leading Edge, **18**, no. 4, 438–452, http://dx.doi.org/10.1190/1.1438307.
Daley, R. M., E. C. A. Gevers, G. M. Stampfli, D. J. Davies, C. N. Gastaldi, P. A. Ruijtenberg, and G. J. O. Vermeer, 1989, Dip and azimuth displays for 3-D seismic interpretation: First Break, **7**, no. 3, 86–95.
Dereshowitz, W. S., M. G. Cottrell, D. H. Lim, and T. W. Doe, 2010, A discrete fracture network approach for evaluation of hydraulic fracture stimulation of naturally fractured reservoirs: 44th US Rock Mechanics Symposium, ARMA, Expanded Abstracts, 10–475.
Dorn, G. A., 2011, Advances in "true volume" interpretation of structure and stratigraphy in 3D volumes: CSEG Recorder, **36**, 9–15.
Espersen, T. B., T. V. Veggeland, J. M. Pedersen, and K. B. Rasmussen, 2000, The lithology cube, 70th Annual International Meeting, SEG, Expanded Abstracts, 643–646.
Gardner, G. H. F., L. W. Gardner, and A. R. Gregory, 1974, Formation velocity and density-the diagnostic basis of stratigraphic traps: Geophysics, 39, no. 6, 770–780, http://dx.doi.org/10.1190/1.1440465.
Gazdag, J., 1978, Wave-equation migration with the phase-shift method: Geophysics, **43**, no. 7, 1342–1351, http://dx.doi.org/10.1190/1.1440899.
Gersztenkorn, A. and K. J. Marfurt, 1999, Eigenstructure-based coherence computations as an aid to 3-D structural and stratigraphic mapping: Geophysics, **64**, no. 5, 1468–1479, http://dx.doi.org/10.1190/1.1444651.
Goldberg, I. and B. Gurevich, 1998, A semi-empirical velocity –porosity clay model for petrophysical interpretation of P- and S-velocities: Geophysical Prospecting, **46**, no. 3, 271–285, http://dx.doi.org/10.1046/j.1365-2478.1998.00095.x.
Gray, F. D. and K. J. Head, 2000, Fracture detection in the Manderson Field: A 3D AVAZ case history: The Leading Edge, **19**, no. 11, 1214–1221, http://dx.doi.org/10.1190/1.1438508.
Haas, A. and O. Dubrule, 1994, Geostatistical inversion—A sequential method of stochastic reservoir modeling constrained by seismic data: First Break, **12**, no. 11, 561–569.
Han, D., A. Nur, and D. Morgan, 1986, Effects of porosity and clay content on wave velocities in sandstones: Geophysics, **51**, no. 11, 2093–2107, http://dx.doi.org/10.1190/1.1442062.
Hennings, P. H., J. E. Olson, and L. B. Thompson, 2000, Combining outcrop data and three-dimensional structural models to characterize fractured reservoirs: An example from Wyoming: AAPG Bulletin, **84**, 830–849.
Herron, D., 2000, Pitfalls in seismic interpretation: Depth migration artifacts: The Leading Edge, **19**, no. 9, 1016–1017, http://dx.doi.org/10.1190/1.1438756.
Hunt, L., S. Reynolds, T. Brown, S. Hadley, J. Downton, and S. Chopra, 2010, Quantitative estimate of fracture density variations in the Nordegg with azimuthal AVO and curvature: A case study: The Leading Edge, **29**, no. 9, 1122–1137, http://dx.doi.org/10.1190/1.3485773.
Hunt, L., J. Downton, S. Reynolds, S. Hadley, D. Trad, and M. Hadley, 2010b, The effect of interpolation on imaging and AVO: A Viking case study: Geophysics, **75**, no. 6, WB265–WB274, http://dx.doi.org/10.1190/1.3475390.
James, H., E. Ragoza, and T. Rastrova, 2011, New method of volume rendering applied to a seismic dataset of the Barnett Shale: GCSSEPM 31st Annual Bob. F. Perkins Research Conference, 208–229.
Jenner, E., 2002, Azimuthal AVO: Methodology and data examples: The Leading Edge, **21**, no. 8, 782–786, http://dx.doi.org/10.1190/1.1503184.
Jianming, T., H. Yue, X. Xiangrong, J. Tinnin, and J. Hallin, 2009, Application of converted-wave 3D/3C data for fracture detection in a deep tight-gas reservoir: The Leading Edge, **28**, no. 7, 826–837, http://dx.doi.org/10.1190/1.3167785.
Johnson, W. E., R. O. Louden, D. D. Lehman, and D. L. Edwards, 2001, Seismic has its multiple attributes, AAPG Explorer.
Knobloch, C., 1982, Pitfalls and merits of interpreting color displays of geophysical data: 52nd Annual International Meeting, SEG, Expanded Abstracts, 112–112.
Kormylo, J. and J. M. Mendel, 1983, Maximum likelihood seismic deconvolution: IEEE Transactions on Geoscience and Remote Sensing, IT-28, 482–488.
Lavergne, M., 1975, Pseudo-diagraphics de Vitesse en offshore profonde: Geophysical Prospecting, **23**, no. 4, 695–711, http://dx.doi.org/10.1111/j.1365-2478.1975.tb01554.x.
Lindseth, R. O., 1976, Seislog process uses seismic reflection traces: Oil & Gas Journal, **74**, 67–71.
Lindseth, R. O., 1979, Synthetic sonic logs—A process for stratigraphic interpretation: Geophysics, **44**, no. 1, 3–26, http://dx.doi.org/10.1190/1.1440922.
Liner, C., 2008, Seismic development 1956–2008: AAPG Explorer, September issue.
Luo, Y., W. G. Higgs, and W. S. Kowalik, 1996, Edge detection and stratigraphic analysis using 3-D seismic data: 66th Annual International Meeting, SEG, Expanded Abstracts, 324–327.
Mallick, S. and P. Ng, 1995, A comparison of poststack and prestack inversion of seismic data, 65th Annual International Meeting, SEG, Expanded Abstracts, 651–654.
Mallick, S., 1999, Some practical aspects of prestack waveform inversion using a genetic algorithm: An example from the east Texas Woodbine gas sand: Geophysics, **64**, no. 2, 326–336, http://dx.doi.org/10.1190/1.1444538.
Mallick, S., 2001, Prestack waveform inversion using a genetic algorithm-The present and the future: CSEG Recorder, **26**, no. 2, 78–84.
Marfurt, K. J., R. L. Kirlin, S. L. Farmer, and M. S. Bahorich, 1998, 3-D seismic attributes using a semblance-based coherency algorithm: Geophysics, **63**, no. 4, 1150–1165, http://dx.doi.org/10.1190/1.1444415.
Marfurt, K. J. and J. Rich, 2010, Beyond curvature—volumetric estimates of reflector rotatiuon and convergence: 81st Annual International Meeting, SEG, Expanded Abstracts, 1467–1472.
Marfurt, K. J. and R. L. Kirlin, 2001, 3-D broad-band estimates of reflector dip and amplitude: Geophysics, **65**, no. 1, 304–320, http://dx.doi.org/10.1190/1.1444721.
Mavko, G., T. Mukerji, and J. Dvorkin, 2003, The rock physics handbook: Cambridge University Press.
Meldahl, P., R. Heggland, B. Bril, and P. de Groot, 1999, The chimney cube, an example of semi-automated detection of seismic objects by directive attributes and neural networks: Part I; methodology: 69th Annual International Meeting, SEG, Expanded Abstracts, 931–934.
Michelena, R. J., E. Gonzales, and P. M. de Capello, 1998, Similarity analysis: A new tool to summarize seismic attributes information: The Leading Edge, **17**, 545–548, http://dx.doi.org/10.1190/1.1438010.
Michelena, R. J., K. S. Godbey, and P. E. Rodrigues, 2011, Facies probabilities from multidimensional crossplots of seismic attributes: Applications to tight gas fields Jonah and Mamm Creek: GCSSEPM 31st Annual Bob. F. Perkins Research Conference, 776–805.

Misra, S. and S. Chopra, 2010, Phase stability via non-linear optimization: A Case study: The Leading Edge, **29**, no. 11, 1138–1343, http://dx.doi.org/10.1190/1.3517304.

Murray, G. H. Jr., 1964, Quantitative fracture study-Sanish Pool, McKenzie County, North Dakota: AAPG Bulletin, **52**, 57–65.

Oldenburg, D. W., T. Scheuer, and S. Levy, 1983, Recovery of the acoustic impedance from reflection seismograms: Geophysics, **48**, no. 10, 1318–1337, http://dx.doi.org/10.1190/1.1441413.

Partyka, G., J. Gridley, and J. Lopez, 1999, Interpretational applications of spectral decomposition in reservoir characterization: The Leading Edge, **18**, no. 3, 353–360, http://dx.doi.org/10.1190/1.1438295.

Poupon, M., J. Gil, M. Hattori, and C. Corbett, 2004, Tracking tertiary delta sands (Urdaneta West, Lake Maracaibo, Venezuela): An integrated seismic facies classification workflow: The Leading Edge, **24**, no. 9, 909–914, http://dx.doi.org/10.1190/1.1803502.

Pramik, B., 2011, Broadband land acquisition—Survey design issues, 82nd Annual International Meeting, SEG, Expanded Abstracts, 4344–4348.

Purves, S. and H. Basford, 2011, Visualizing geological structure with subtractive color blending: GCSSEPM Conference.

Raymer, L. L., E. R. Hunt, and J. S. Gardner, 1980, An improved sonic transit-time porosity transform: SPWLA, 21st Annual Logging Symposium, Transactions, Paper P.

Reine, C. A. and R. B. Dunphy, 2011, Weighing in on the seismic scale: The use of seismic fault measurements for constructing Discrete Fracture Networks in the Horn River Basin: CSPG/CSEG/CWLS Convention, 1–4.

Rijks, E. J. H. and J. C. E. M. Jauffred, 1991, Attribute extraction: An important application in any detailed 3D interpretation study: The Leading Edge, **10**, no. 9, 11–19, http://dx.doi.org/10.1190/1.1436837.

Roberts, A., 2001, Curvature attributes and their application to 3-D interpreted horizons: First Break, **19**, no. 2, 85–99, http://dx.doi.org/10.1046/j.0263-5046.2001.00142.x.

Roy, A., M. Matos, and K. J. Marfurt, 2011, Application of 3D clustering analysis for deep marine seismic facies classification—an example from deep water northern Gulf of Mexico: GCSSEPM 31st Annual Bob. F. Perkins Research Conference, 410–439.

Schneider, W. A., 1978, Integral formulation for migration in two and three dimensions: Geophysics, **43**, no. 1, 49–76, http://dx.doi.org/10.1190/1.1440828.

Sonneland, L., O. Barkved, M. Olsen, and G. Snyder, 1989, Application of seismic wave-field attributes in reservoir characterization: 59th Annual International Meeting, SEG, Expanded Abstracts, 813–817.

Staples, E. and K. Marfurt, 2011, Quantitative curvature calibration from clay model experiments: 82nd Annual International Meeting, Society of Exploration Geophysics, Expanded Abstracts, 1908–1912.

Strecker, V. and R. Uden, 2002, Data mining of 3D poststack seismic attribute volumes using Kohonen self-organizing maps: The Leading Edge, **21**, no. 10, 1032–1037, http://dx.doi.org/10.1190/1.1518442.

Stolt, R. H., 1978, Migration by Fourier transform: Geophysics, 43, no. 1, 23–48, http://dx.doi.org/10.1190/1.1440826.

Taner, M. T., F. Koehler, and R. E. Sheriff, 1979, Complex seismic trace analysis: Geophysics, **44**, no. 6, 1041–1063, http://dx.doi.org/10.1190/1.1440994.

Thompson, A., 2011, Induced fracture detection in the Barnett Shale, Ft. Worth Basin, Texas: M.S. Thesis, University of Oklahoma.

Thomsen, L., 1986, Weak elastic anisotropy: Geophysics, 51, no. 10, 1954–1966, http://dx.doi.org/10.1190/1.1442051.

Todorovic-Marinic, D., S. Chopra, and M. Edmonds, 2011, Advanced seismic techniques help in characterizing a challenging Jean Marie carbonate play, NE British Columbia, Canada—a Case Study: CSEG Recorder, **37**, 50–59.

Tonn, R., 2002, Neural network seismic reservoir characterization in a heavy oil reservoir: The Leading Edge, 21, no. **3**, 309–312, http://dx.doi.org/10.1190/1.1463783.

Trad, D., 2009, Five dimensional interpolation: Geophysics, **74**, no. 6, V123–V132, http://dx.doi.org/10.1190/1.3245216.

Vail, P. R., R. M. Mitchum Jr., and S. Thompson III, 1977, Seismic stratigraphy and global changes of sea level, Part 4: Global cycles of relative changes of sea level, in C. E. Payton, eds., Seismic stratigraphy applications to hydrocarbon exploration: AAPG Memoir, **26**, 83–97.

Whitcombe, D., 2002, Elastic impedance normalization: Geophysics, **67**, no. 1, 60–62, http://dx.doi.org/10.1190/1.1451331.

Wyllie, M. R. J., A. R. Gregory, and L. W. Gardner, 1956, Elastic wave velocities in heterogeneous and porous media: Geophysics, **21**, no. 7, 41–70, http://dx.doi.org/10.1190/1.1438217.

Williams, M. and E. Jenner, 2002, Interpreting seismic data in the presence of azimuthal anisotropy or azimuthal anisotropy in the presence of seismic interpretation: The Leading Edge, 21, no. 8, 771–774, http://dx.doi.org/10.1190/1.1503192.

Xu, Y. and S. Chopra, 2008, Deterministic mapping of reservoir heterogeneity in Athabasca oil sands using surface seismic data: The Leading Edge, **27**, no. 9, 1186–1191, http://dx.doi.org/10.1190/1.2978981.

Acknowledgments: We thank Arcis Seismic Solutions for permission to show the data examples as well as for the permission to publish this work. We also thank Ritesh Sharma for his help in processing the data shown in Figure 6. We gratefully appreciate the review comments that we received from Alistair Brown, Don Herron, Niranjan Nanda, Lee Hunt, and Scott Reynolds, which helped improve the quality of the paper.

Corresponding author: schopra@arcis.com